Drilling Mechanism of Autonomous Burrowing Robot for Lunar Subsurface Exploration

Kenji NAGAOKA[*1], Takashi KUBOTA[*2], Ichiro NAKATANI[*2], Satoshi TANAKA[*2]
[*1]*The Graduate University for Advanced Studies,* [*2]*JAXA/ISAS*
E-mail:nagaoka@nnl.isas.jaxa.jp

Abstract

Lunar and planetary subsurface exploration is of considerable significance. The authors have studied the strategies for subsurface excavation and propulsion for the development of a lunar subsurface explorer. The authors have proposed an autonomous robotic explorer which can burrow into the soils. Based on the strategies the authors have already considered, this paper especially focuses on the excavation mechanism of a robotic system for near-future lunar subsurface exploration. The main objective of the proposed robot is to bury a scientific observation instrument like a long-term seismometer under the lunar surface, which is covered with very compacted lunar regolith. Therefore, an efficient excavation mechanism is required. In this paper, the authors propose a new screw drilling system with double rotation, which is called N-RDM (Non-Reaction Drilling Mechanism). Through some experiments and analyses, this paper discusses the feasibility and effectiveness for the proposal of a burrowing robot system.

1 Introduction

Since the creation of time, the Moon is one of most attractive celestial bodies for human beings. The outcomes of the Apollo missions by the U.S. is particularly recognized as significant achievement in space development [1]. Many countries have tried to improve upon it. From various sample returns and measurements, a lot of important knowledge has been gained in lunar and space science. However, the Moon still has a lot of unanswered questions such as its origin, chemical components, and internal structure. To answer these questions, it is required to obtain global information about the Moon in future lunar exploration missions. Therefore, the authors propose a robotic system for burying a scientific observation equipment like a long-term seismometer under the surface to investigate the internal of the Moon (Fig.1). In general, the lunar surface is covered with very fine soils, called lunar regolith, and the lunar regolith has high adiabatic property. Given this, the instruments buried in the lunar regolith can be kept at a constant temperature, even at night. To accomplish this, some scientists say that the instrument should be placed about 1 meter below the surface. Consequently, this enables it to function for a long time without any heaters. Also, the buried seismometer can realize better contact with the surrounding lunar regolith, so it would be able to capture very small lunar seism. This paper first describes the strategies for subsurface propulsion of a burrowing robotic system and its required mechanisms. Then, this paper especially discusses the excavation mechanism, which is very important for such a system. Finally the authors propose a novel excavating mechanism that is suitable for a burrowing robot, and present the results of some experiments.

2 Burrowing Robot

2.1 Subsurface mobile robots

So far, there have been numerous researches of robots with a locomotion mechanism. But, most of them have paid attention to just only mobility. There are several environments for movement, such as on the ground, inside of tubes, and under water. Meanwhile, some have developed biomimetic robots that can move like underground creatures, for instance an earthworm or a snake, and their locomotion is mostly restricted to the above. However, studies on autonomous robots that can move underground are especially rare. That is because soils are too complex and unsteady as a locomotion environment. Also, any such study would need to consider both the locomotion and how to generate the space for locomotion.

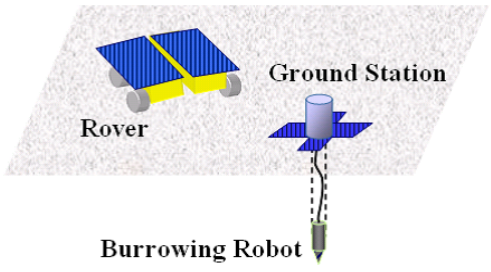

Fig.1: Lunar subsurface exploration mission

Table 1: Planetary excavation systems

	mechanism	size	weight	robustness	purpose
Bucket Wheel	*simple*	*large*	*heavy*	×	*sampling*
Penetrator	*simple*	*middle, long*	*middle*	×	*investigation*
Drill	*simple*	*narrow, long*	*light*	○	*sampling*
Burrowing Robot	*complex*	*compact*	*light*	△	*investigation*

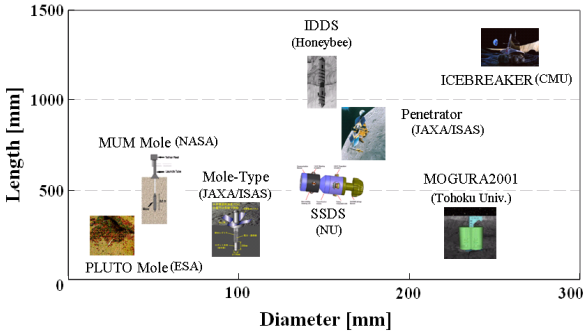

Fig.2: Overview of planetary excavating robots

2.2 Conventional robots for planetary subsurface exploration

Planetary exploration with excavation of soils has received a lot of attention in the world. Table 1 shows a comparison of planetary excavation systems. Here, the robustness refer to the capability to have different excavating opportunities. So far, there have been proposal for digging robots for planetary subsurface exploration [2]-[6]. However, it would be hard for these robots to bury a large instrument such as a seismometer. An overview of some proposed ideas which are classified by length and diameter is shown in Fig.2. The ICEBREAKER of CMU and the Lunar-A penetrators of JAXA are not actually autonomous burrowing robots, but robotic systems for subsurface investigation or a similar objective. Hence, these two different methods are included in Fig.2 for comparison.

2.3 Strategies for subsurface propulsion

Based on the past researches, the authors set the following assumptions:

- The burrowing robot is carried by the rover
- Power is supplied by a cable from the ground station
- Target depth is several meters from the surface
- Target soil-layer is lunar regolith
- The robot diameter is about 0.1 m
  (The seismometer's diameter: about 0.05 m)

Next, the authors define two phases for subsurface propulsion by a burrowing robot, and consider different strategies for each phase as follows.

1. Make space

- Compress regolith
- Remove and back transport regolith

2. Advance forward

- Utilize contact with surrounding regolith
- Utilize excavated regolith
- Self advancing without utilizing regolith

Now there are different ways to achieve the above strategies [7], and the proposed robots shown in Fig.2 can be classified by these strategies.

By applying Apollo's data regarding compression index [1], the authors have previously concluded that it would be unlikely that the regolith can be compressed for making space. Also the authors concluded quantitatively by applying the rankine's soil pressure theory that a burrowing robot needs to generate a propulsive force [7]. Therefore, from the next section this paper describes a concrete excavating mechanism and uses it as a baseline.

3 Screw Drilling Mechanism

The earth-auger method is a screw mechanism used in excavation systems on Earth. According to the referense [8], the screw drilling state can be in one of the following 3 states.

⟨1⟩ Auger moves forward one pitch forward after one rotation, soils are not excavated, and there is no shear on the edges of the screw.

⟨2⟩ Auger moves forward less than one pitch forward after one rotation, and soils are excavated and transported backward.

⟨3⟩ Auger cannot move forward at all despite rotation.

In general, the state of an earth-auger is in the state ⟨2⟩. This paper also assumes this state. This excavating mechanism using a helical screw is one of the major methods in the field of construction and civil

engineering. The shapes of these helical screws is determined by past empirical knowledge. The action performance is the almost completely controlled by operation, and there have been very few theoretical studies. The method involves human beings and large scale systems in order to treat the behavior of complicated soils. Some researchers focus on the estimation of discharging soils and the description of the dynamics [9]. The results indicate a very good estimation, but the objective is limited to such discharging estimation and some theoretical considerations are lacking.

Another use of screw mechanism is in screw piles. The application is for improving soft ground, as a countermeasure against liquefaction almost all of the researches are focused on the bearing capacity. Additionally, like the earth-auger its mechanism is not clearly understood.

A third use of the screw mechanism is found in systems for conveying materials. These researches are principally focused on the screw conveyors, which transport materials obliquely upward, so it is hard to apply the concept to a burrowing robot system.

From these, the authors have decided to do some basic experiments for the analysis and clarification of the behavior of the screw excavating mechanism.

4 Non-Reaction Mechanism

4.1 Proposal of Double Rotation System

With the above considerations, the required properties for a robotic excavation mechanism are the following:

- Fore-soil removal and transportation backward
- Generation of propulsive force
- Dust prevention mechanism

Therefore, a screw drill, which has a series of spiral wings, is one of candidates. However, a serious problem is that a single spinning drill results in a reaction force to the body. This reaction can generate the friction between the body and the supporting soil reducing the drilling efficiency. It can also lead to the wobbling of the propulsion axis. This paper proposes a new type of spiral screw drill unit as a novel excavation mechanism to improve this problem.

A mechanism using double rotations already exists as the doughnut-auger method. It has two rotating parts, an inner-screw and an outer-casing. The mechanisms of the reaction reduction have not been studied so well. Thus, it cannot effectively reduce the reaction. An outer-casing for reducing the reaction is very useful for drilling a hole, but it increases the number of driven parts, which means an increase in power consumption. It is also structural redundant for a burrowing robot. Due to these factors the authors develop a new screw mechanism with N-RDM (Non-Reaction Drilling Mechanism) by separating the screw parts, and applied it to a burrowing robot. Here, the double rotation methods are classified into three types as shown in Fig.3. The contra-rotor type (a) has one drilling unit which has the contra-rotation axis at coincident with the rotation axis. The twin-rotor type (b) consists of two drilling units whose rotation axes are fixed and parallel to each other. The dual-spin type (c) has one drilling unit whose rotation axis is spinning around another spin axis. Each type has two rotation axes, so it is possible to cancel the reaction. However, there are some notable differences. Firstly, the contra-rotor type (a) is compact in size, and it can be estimated that it would have an equivalent excavating performance with the single screw drilling mechanism. Secondly, the twin-rotor type (b) has an unexcavated space between the two drilling units, resulting in an anomalous shape. It is impossible to make one circular hole, and a constraint on the body shape must be considered. Thus, it can be estimated that it would have lower efficiency. Thirdly, the dual-spin type (c) has a driven part not used for drilling, so the efficiency would be ever lower. According to these considerations, the authors adopt the contra-rotor type and will do some experiments in the near future.

(a) Contra-rotor (b) Twin-rotor (c) Dual-spin

Fig.3: Double rotation screws

4.2 SSD

The schematic of the basic model, which is called SSD (Single Screw Drilling) unit, is represented in Fig.4(a). Also Fig.4(b) shows the prototype. The developed SSD is a conceptual model of the contra-rotor type screw, and it serves as a basic dynamics model for theoretical analysis.

The SSD unit consists of a body part and an excavation part. Furthermore, the excavation part has an inner cone, called CONE, and a helical screw wing which winds around the CONE, called SCREW. As shown in Fig.4, α_{SC}[rad] denotes the angle of inclination of the SCREW 's center position and p[m] denotes the SCREW's variable pitch. The screw length is L[mm], and the maximum screw diameter is D[mm]. In general, the SCREW model can be mathematically expressed as a function of a logarithmic spiral.

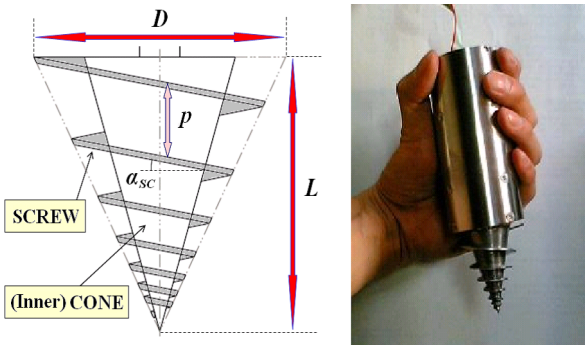

(a) Simplified model (b) Prototype

Fig.4: SSD unit

4.3 Contra-rotor

Figure 5(b) shows the prototype of a new contra-rotor screw, which the authors developed. This prototype consists of the body, the front screw and the rear screw. The two screws can be driven independently by separated motors to analyze the behavior. Also Fig.5(a) represents the schematic. From this the length of the front and the rear screw is both $L/2$, the front's diameter is $D/2$, the rear's diameter is D, and the ratio between the moment of inertia between the front and the rear is approximately 1:31.

4.4 Basic experiments

4.4.1 Experimental set-up

Some experiments with the SSD and the contra-rotor screw have been carried out as shown in Fig.6. Also in the experiment, the soil is silica sand and the specifications are shown in Table 2. The front screw and the rear screw of the contra-rotor are independently controlled. The starting situation is that the screw is completely buried and the body stands out on the surface, and the propulsive force comes from just its weight. Through the experiments, the encoder value which indicates motor rotation speeds, the active time and the average sinkage are measured, and the average penetration speed is calculated.

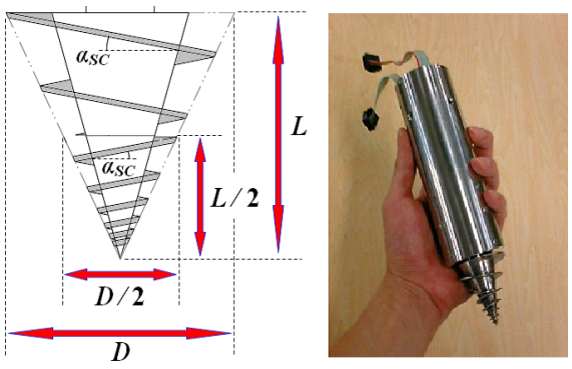

(a) Simplified model (b) Prototype

Fig.5: Contra-rotor screw unit

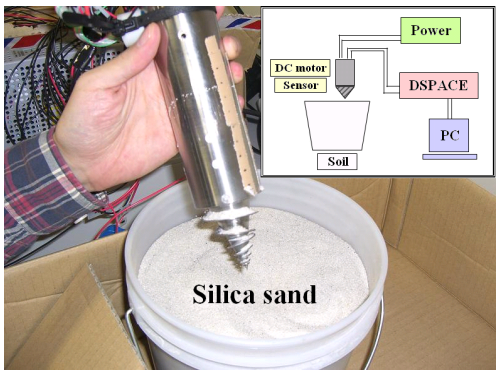

Fig.6: Experimental environment

4.4.2 Drilling performance: *SE*

The *Specific Energy*, which is called *SE*, is a major index of drilling performance [10]. In this paper, the authors evaluate the excavating properties by applying this index. The required energy per minute, E[MJ/min], is calculated as follows.

$$E = W \times \pi D \times f \times 10^{-9} \quad (1)$$

$$W = w_1 \times g + w_2 \quad (2)$$

where, D[mm] is the diameter of hole, f[rpm] is the rotation speed, W[N] is propulsive force, w_1[kg] is the robot mass, g[m/s^2] is the gravity acceleration and w_2[N] is all external forces without the weight. Here, the volume of the soil removed per minute, V[m^3/min], is calculated by using the penetration speed PR[m/hr] as following.

$$V = \pi \times \left(\frac{D \times 10^{-3}}{2}\right)^2 \times \frac{PR}{60} \quad (3)$$

Thus, SE[MJ/m^3] is defined by the following equation.

$$SE = \frac{E}{V} = \frac{0.24 \cdot f}{D \cdot PR} \cdot (w_1 g + w_2) \quad (4)$$

From the above equation (4), an increase in SE means that its performance becomes lower.

4.4.3 Equivalent angular velocity

To apply the evaluation equation (4), an equivalent angular velocity of the double rotation screw is considered. By equating the rotating energies, the equivalent angular velocity ω_S[rad/s] is derived. Here, the

Table 2: Specifications of screw units

	L	D	Mass	α_{SC}
SSD	50 mm	50 mm	356-867 g	10 deg
Contra-Rotor	50 mm	50 mm	604 g	10 deg

total energy of rotations is described as follow, neglecting the body's rotation.

$$\frac{1}{2}I_1\omega_1^2 + \frac{1}{2}I_2\omega_2^2 = \frac{1}{2}(I_1 + I_2)\omega_S^2 \quad (5)$$

where, I_1[kgm^2] is the moment of inertia of the front screw, I_2[kgm^2] is the moment of inertia of the rear screw, ω_1[rad/s] is the angular velocity of the front screw and ω_2[rad/s] is the angular velocity of the rear screw. Hence, from the above, ω_S is derived by the following equation.

$$\omega_S = \sqrt{\frac{I_1\omega_1^2 + I_2\omega_2^2}{I_1 + I_2}} \quad (6)$$

Through the experiments, ω_S [rad/s] can be converted to the rotation speed as following in order to utilize the above equation (4). Also, the ratios of the angular velocities and the rotation speed between screws are both defined as follows.

$$K = \frac{\omega_1}{\omega_2} = \frac{f_1}{f_2} \quad (7)$$

5 Experimental Results

5.1 Results: Non-reaction

When the SSD driven only the body rotates while the remain in place due to the frictional resistance from the soil against the screw. It is not really an excavation or propulsion mode, and the result of the SSD unit indicates the SSD is unsuitable for a burrowing robot. In contrast, a reduction of the body rotation is confirmed in the case of the contra-rotor screw. Also, the non-reaction condition is confirmed at around K=60. On the other hand, slight wobbling motion of the body was observed even near the non-reaction condition. This could be the effect of by the connecting cords or the mass decentering. Alternatively, the wobbling could also arise from the skew symmetry of the screw. This could be resolved by using a dual spiral structure. The authors plan to do more experiments for measuring the driving torques and consider the theoretical approaches to find out the mechanism. However, the small wobbling behavior is not regarded as a critical problem given the frictional resistance against the body underground.

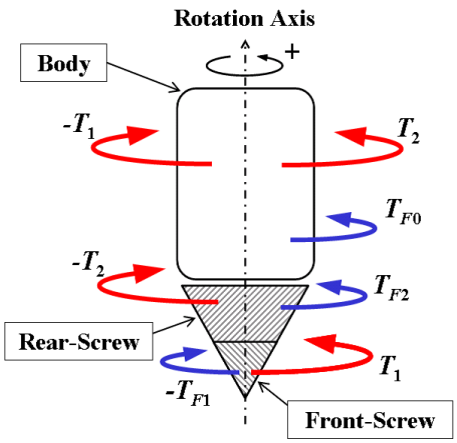

Fig.7: Dynamics model of contra-rotor screw

5.2 Results: *SE*

Figure 8 and 9 show the experimental results. In the case of the SSD, when the body is free the body rotates with any screw rotation. Hence the body is fixed by hands to stop the body reaction in order to measure the drilling properties. As shown in Fig.8(a), *SE* is directly proportional to *W* and would be saturated with increase of *f* in the experiments of the SSD. In Fig.8(a), the blue line denotes the approximate function about *SE* with constant *f* and variable *W*, and the green line indicates average *SE* with constant *W* and variable *f*. The lower performance with increasing *W* is due to the increase of frictional resistance. This is expected because an increase of *W* is proportional to an increase of normal force between the screw and soils below. This fact is confirmed in Fig.8(b), which indicates relationship among *PR*, *W*, and *f*. Given these results, *PR* is directly proportional to *f* which is equal to the angular velocity and *W* has an insignificant effect on *PR* during these experiments. It is obvious that with screw driving with no *W*, propulsion stop. So it is preferable for the burrowing robot to be able to generate arbitrarily an optimal *W*.

Next the results of contra-rotor screw are shown in Fig.9. The body is fixed by hand in Fig.9(a), the body remains free in Fig.9(b), and Fig.9(c) indicates a comparison of the relationship among *SE*, *f* and *PR* in (a) and (b). Also in Fig.9, the horizontal axis represents the ratio *K* as referred to above under the constant *W*, and each line denotes the approximates curve associated with the discrete data of *SE*, *f*, and *K*. As shown in Fig.9(a), the property *SE* is directly proportional to *K*, and also, *PR* and *f* heavily depends on *K* and shows a similar approximate curve. At around *K*=1, *SE* is sustained compared with the SSD data, where the green line is the estimated *SE* of the SSD at the same mass. In other words, the effectiveness is indicated if the non-reaction state could be achieved. On the other hand, although the curves shown in Fig.9(b) is very similar with the curves in Fig.9(a), and it shows an obvious performance reduction at lower *K*. Instead, the non-reaction state is confirmed at around *K*=60, and the performances of Fig.9(a) and Fig.9(b) indicate indeed almost the same value near the non-reaction condition. Therefore, this result indicates the validity of non-reaction mechanism.

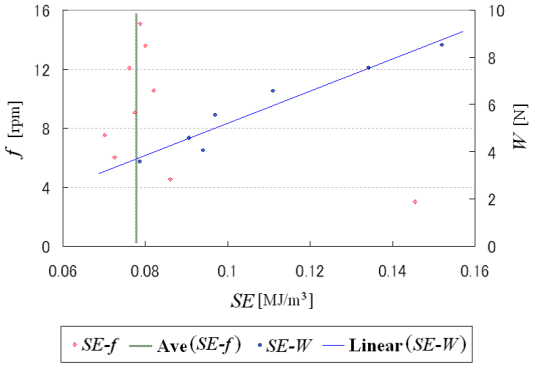

(a) Relationship between *SE*, *f*, and *W*

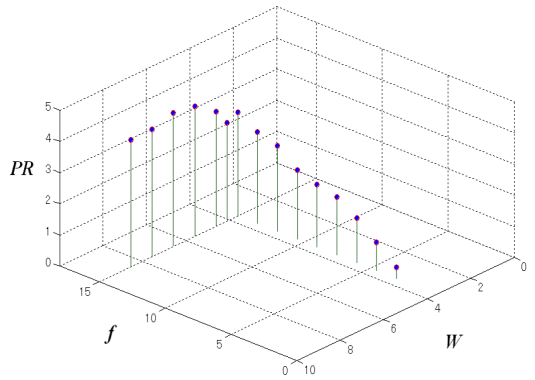

(b) Relationship between *PR*, *f*, and *W*

Fig.8: Experimental results of SSD

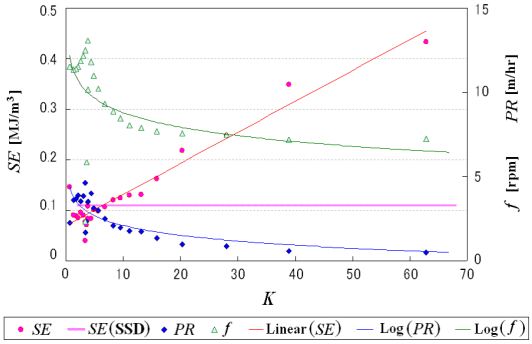

(a) Body fixation

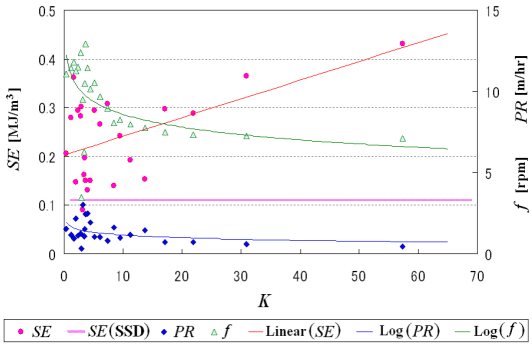

(b) Body free

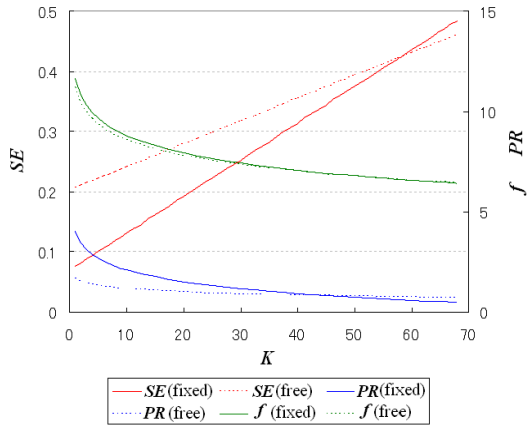

(c) Comparison between the body is fixed and free

Fig.9: Experimental results of contra-rotor screw

5.3 Analysis

According to the above results, the following results are obtained from the experiments:

- The Penetration speed is proportional to the rotation speed
- The best excavating performance condition: K=1
- The Non-reaction condition: around K=60

5.3.1 Equation of rotation

Here, based on the simplified dynamics model as shown in Fig.7, the equations of rotation are defined as follows.

$$I_0\dot{\omega}_0 = -T_1 + T_2 - sgn(\omega_0)\cdot T_{F0} \quad (8)$$

$$I_1\dot{\omega}_1 = T_1 - T_{F1} \quad (9)$$

$$I_2\dot{\omega}_2 = -T_2 + T_{F2} \quad (10)$$

where, I_0[kgm^2] is the moment of inertia of the body, ω_0[rad/s] is the angular velocity of the body, and $sgn(\cdot)$ is a signum function. The angular velocity indicates a positive value when the direction is anticlockwise direction along the rotation axis passing through the center of the robot (Fig.7). Also, T_1[Nm] is the driving torque for the front screw, T_2[Nm] is the driving torque for the rear screw, T_{F0}[Nm] is the frictional torque against the body, T_{F1}[Nm] is the frictional torque against the front screw and T_{F2}[Nm] is the frictional torque against the rear screw. These torques are positive values, irrespective of the rotation directions.

5.3.2 Non-reaction control

Next by using above equations (10), this paper describes the mechanism of canceling the counter-torque against the body. Given the state that the reaction against the body is approximately zero, the work of the friction T_{F0} would be zero. Thus, the driving

torques for the non-reaction are derived as follows.

$$\dot{\omega_0}(t) \to 0 : T_1(t) = T_2(t) \tag{11}$$

On the other hand, when the body rotates, the relationship between the driving torques is expressed as the following equations.

$$\begin{aligned} \omega_0(t + \Delta t) &= \omega_0(t) + \dot{\omega_0}(t) \cdot \Delta t \to 0 \\ \therefore T_1(t) - T_2(t) &= \frac{I_0 \omega_0}{\Delta t} + sgn(\omega_0) \cdot T_{F0} \end{aligned} \tag{12}$$

Here, Δt is the cycle of the input torque, and the relationship between torques would be described in the case of controlling the body's small reaction within one cycle input.

5.3.3 Evaluation of DC motor

The electric properties of a DC motor are calculated as follows.

$$V_M = I_M \cdot R_M + k_e \cdot \omega + V_B \tag{13}$$

$$T = k_t \cdot I_M \tag{14}$$

where, V_M[V] is the input power, I_M[A] is the electric current of the motor, R_M[Ω] is the electric resistance of the motor with the internal resistance, k_e[Vs/rad] is the factor of counter electromotive force, ω[rad/s] is the directed relative angular velocity, V_B[V] is the voltage drop by the friction of the brush, T[Nm] is the driving torque, k_t[Nm/A] is the torque constant. Where, the no-load current of the motor is ignored. In fact, k_e is really equal to k_t and V_B by the metallic brush has almost negligible V_B, hence the above equation (13) is rewritten as follows.

$$V_M = I_M \cdot R_M + k_e \cdot \omega \tag{15}$$

Also from an absolute coordinate, the motor stator's directed angular velocity is ω_{sh}[rad/s] and a motor shaft's directed angular velocity is ω_{sh}[rad/s]. So the ω is defined as following.

$$\omega = \omega_{sh} - \omega_{st} \tag{16}$$

In general, the relationship between the motor torque and the angular momentum H[kgm^2/s] is written as follows.

$$T = \dot{H} = I_{sh}\dot{\omega}_{sh} - I_{st}\dot{\omega}_{st} \tag{17}$$

where, I_{sh}[kgm^2] is the moment of inertia of the motor shaft and I_{st}[kgm^2] is the moment of inertia of the motor body including the stator. Thus, from these considerations, T is calculated as follows.

$$T = k_e \cdot \frac{V_M - k_e \cdot \omega}{R_a} \tag{18}$$

From the above considerations, Figure 10 shows the simulation result of an example indicating the DC motor characteristic. Here, the input voltage V_M is assumed to be constant and the values regarding the frictional resistances, which are given with the ratio between the surface area of the body and the screw, assume much smaller than the torques. According to Fig.10, the frictional resistance reduce directly the motor's rotation speed with a constant voltage. Therefore the output torque depends on the higher friction, but the another rotation speed keeps accelerating until the driving torque would be equal to the resistance torque.

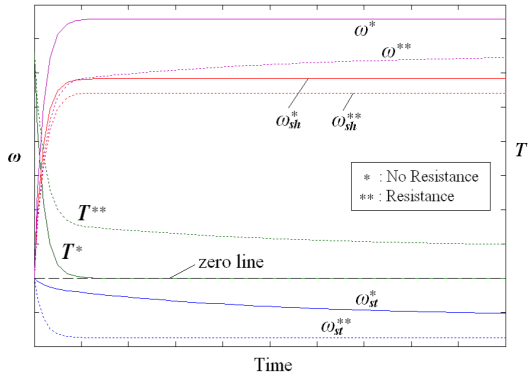

Fig.10: Simulation result of DC motor characteristic

In these experiments, the non-reaction state is indeed observed as a value around K=60. However, based on a theoretical analysis, given no-load state K would be due around 105 with the gear reduction ratio, the moment of inertia and the voltage. Where, the gear reduction ratio of the front screw is 1.875 and the rear one is 0.5. The ratios are indeed not equivalent values to f in Fig.8 or 9. Thereby, the effects of frictional resistance reduce the rotation speed or K as above considered. Even the ratio between surface areas of screws assumes 1:3, the differential can become a critical problem for the control. There could be several other factors, but the most dominating factor is the frictional resistance. The tendency depends on the frictional resistance, and more considerations are required with the theoretical analysis. Thus, the theoretical approaches are significant future works for analysis of the soil frictional resistance against the screw motion during the driving of the burrowing robot.

5.3.4 Sustaining the drilling performance

To sustain the excavating performance SE, or produce the required propulsive speed PR, the control of K is necessary as mentioned above. The control law also depends on the friction conditions. With the non-reaction control, the absolute values of each motor torque retain same. In other words, the absolute angular accelerations of the motors depend on the torque history and the frictional resistances which include a uncertainty. So it is surely needed to make the hybrid control law with the non-reaction and the performance sustainment, and that is our future work.

6 Conclusion

In this paper, the authors have discussed an autonomous burrowing robot system for the lunar subsurface exploration. The authors especially proposed a novel excavation mechanism, called contra-rotor screw with N-RDM, for the development of the burrowing robot for lunar subsurface exploration. In particular, this paper has presented the important and basic guideline concerning a relationship among the penetration speed, the rotation speed, the propulsive force and the total performance *SE*. And then the authors have indicated the feasibility and the effectiveness through some experimental analyses. Some experiments for the validation of the proposed excavating method are listed as future works. Also, further theoretical analysis of the screw mechanism for excavating soils and its hybrid control law are in progress.

Acknowledgments

Dr. Otsuki, who is an assistant professor at ISAS/JAXA, supported the experiments. Mr.Edmondo, who is a doctoral course student in the laboratory, helped in writing this paper. Here, the authors would like to express my appreciation for them.

References

[1] G. Heiken, D. Vaniman and B. French, "*Lunar Sourcebook*", Cambridge University Press, 1991.

[2] K. Watanabe, S. Shimoda, T. Kubota and I. Nakatani, "A Mole-Type Drilling Robot for Lunar Subsurface Exploration", *Proc. of the 7th iSAIRAS*, AS-7, 2003.

[3] K. Yoshida, N. Mizuno, T. Yokoyama, Y. Kanamori, M. Sonoyama and T. Watabe, "Development of Mole-type Robot for Lunar/Planetary Sub-Surface Exploration, and its Performance Evaluation" (in Japanese), *Proc. of the 20th Annual Conf. of the RSJ*, 1J35, 2002.

[4] Y. Liu, B. Weinberg and C. Mavroidis, "Design and Modeling of the NU Smart Space Drilling System (SSDS)", *Proc. of the 10th ASCE Aerospace Division International Conf. on Engineering, Construction and Operations in Challenging Environments (Earth and Space 2006)*, 2006.

[5] R. Campaci, S. Debei, R. Finotello, G. Farziano, C. Bettanini, M. Giacometti, G. Rossi, G. Visentin and M. Zaccariotto, "Design and Optimization of A Terrestrial Guided Mole for Deep Subsoil Exploration-Boring Performance Experimental Analysis", *Proc. of the 8th iSAIRAS*, 2005.

[6] S. P. Gorevan, T. M. Myrick, C. Batting, S. Mukhrrjee, P. Bartlet and J. Wilson, "Strategies for Future Mars Exploration: An Infrastructure for The Near and Longer Term Future Exploration of The Subsurface of Mars", *Proc. of the 6th Int. Conf. on Mars*, 2003.

[7] K. Nagaoka, S. Tanaka and T. Kubota, "Study on Excavation Mechanism for Lunar Subsurface Exploration by Burrowing Robot", *Proc. of the 17th Workshop on Astrodynamics and Flight Mechanics*, C-21, 2007.

[8] The Society of Geotechnical Engineering ed., "*Soil Mechanics and Foundation Engineering -Recent construction methods-*" (in Japanese), The Society of Geotechnical Engineering, 1967, pp.11-13.

[9] H. Fukada, M. Ootsuka, Y. Tanaka and Y. Shioi, "Discharging Characteristics by Screw Auger of Gravel Drain Pile" (in Japanese), *JSCE J. of Construction Engineering and Management*, Vol.62, No.2, 2006, pp.203-212.

[10] H. Raiba, "Specific Energy as a Criterion for Drill Performance Prediction", *Int. J. of Rock Mech. Min. Sci. and Geomech. Abstract*, Vol.19, 1982, pp.39-42.